Journal of Alloys and Compounds 505 (2010) 501–504

Contents lists available at ScienceDirect

Journal of Alloys and Compounds

journal homepage: www.elsevier.com/locate/jallcom

Deformation behaviors of a TiZrNiCuBe bulk metallic glass under shock loading

Svetlana A. Atroshenko[a], N.F. Morozov[b], W. Zheng[c], Y.J. Huang[c], Yuri V. Sudenkov[b], N.S. Naumova[b], J. Shen[c,*]

[a] Institute for Problems of Mechanical Engineering, Russia Academy of Science, St. Petersburg, Russia
[b] St. Petersburg State University, St. Petersburg, Russia
[c] School of Materials Science and Engineering, Harbin Institute of Technology, Harbin 150001, China

ARTICLE INFO

Article history:
Received 30 May 2010
Accepted 22 June 2010
Available online 1 July 2010

Keywords:
Bulk metallic glass
Planar impact
Spall strength

ABSTRACT

In the present work, the shock responses of $Ti_{40}Zr_{25}Ni_3Cu_{12}Be_{20}$ bulk metallic glass (BMG) were investigated by using a planar impact technique on an electrical explosion of conductor (EEC) installation. The spallation occurs even if the stress behind the shock front is less than the Hogoniot elastic limit (HEL) stress of the Ti-based BMG. When the velocity of aluminum flyer with thickness of 1.7 mm is 570 m/s, the spall strength of the alloy sample is 2.9 GPa while the stress, strain and particle velocity behind the shock front are 4.3 GPa, 2.8% and 150 m/s, respectively. The calculated yield strength for the alloy upon the dynamic loading is much larger than that under the quasistatic compressive loading. The scanning electron microscope (SEM) observation indicates that, after dynamic loading, the free surface of the sample forms a lot of shear bands and cracks. Optical microscope (OM) shows that cracks and microvoids, which cause the occurrence of the spallation of the sample, are distributed on the cross-section of the recovered Ti-based BMG sample.

1. Introduction

Material behaviors under conditions of high strain rates are of practical importance with the rapid development of military and aerospace technology. Bulk metallic glasses (BMGs), as a class of advanced structural and functional materials, which possess a combination of outstanding properties including ultrahigh strength, high hardness, large elastic limit, unique fracture toughness, and excellent corrosion resistance [1–7], have gradually gained considerable attentions from materials science community. It should be of scientific and technological interest to probe the deformation behaviors of BMGs under plate-impact loading in order to shed lights on the high strain-rate response of this advanced materials and for their great potential applications, such as kinetic energy penetrators. Zhuang et al. [8] firstly studied the shock wave response of $Zr_{41.5}Ti_{13.5}Cu_{12.5}Ni_{10}Be_{22.5}$ BMG using planar impact technique and reported a surprisingly low Hugoniot elastic limit (HEL) (<0.1 GPa). Turneaure and his co-workers [9,10] reported that the HEL stress of $Zr_{56.7}Cu_{15.3}Ni_{12.5}Nb_{5.0}Al_{10.0}Y_{0.5}$ BMG was determined to be 7.1 ± 0.3 GPa, a value quite different with that from Ref. [8]. Togo and co-workers [11,12] stated the HEL stress of $Zr_{55}Al_{10}Ni_5Cu_{30}$ BMG was 6.2 GPa, and a kink, which may be due to the phase transition, could be observed on the Hugoniot compression curve at 14 GPa for the glass. Yuan et al. [13] conducted plate-impact experiments to investigate the shock response of a Zr-based BMG, $Zr_{41.25}Ti_{13.75}Ni_{10}Cu_{12.5}Be_{22.5}$, in the normal stress range of 5–7 GPa. The HEL stress of the BMG was estimated to be 6.15 GPa. The above experiments are of importance to understand the equations of state (EOS), constitutive equations and damage mechanism of bulk glass-forming alloys upon dynamic loading. However, quite limited data are currently available for the dynamic compression properties of Ti-based bulk glassy alloys.

In this paper, shock wave compression experiments were performed on the $Ti_{40}Zr_{25}Ni_3Cu_{12}Be_{20}$ BMG in order to gain better understanding of the response features upon shock loading. Recovery experiment was also carried out in order to investigate the structure of shock-compressed samples.

2. Experimental

Alloy ingots with the nominal composition $Ti_{40}Zr_{25}Ni_3Cu_{12}Be_{20}$ (at.%) were prepared from a mixture of constituent elements with purities better than 99.9% (wt.%), by non-consumable arc melting under a Ti-gettered argon atmosphere. To ensure composition homogeneity, each ingot was remelted at least four times. Bulk glassy samples were prepared by remelting the button ingots and drop casting the molten alloy into a copper mold with an internal cavity of 3 mm × 30 mm × 80 mm. The structure of the plate-shaped samples was identified by X-ray diffraction (XRD) using the Cu Kα radiation.

Before dynamic compression experiments, the elastic characteristics for the glass were measured. Density, ρ_0, of the sample was measured by an Archimedean method and averaged over several samples cut from different positions of each plate. Longitudinal C_l and transverse C_t wave velocities were determined by testing the acoustic signals oscillograms in glassy samples. Elastic constants of the glass were

* Corresponding author. Tel.: +86 451 86402092; fax: +86 451 86403196.
E-mail address: junshen@hit.edu.cn (J. Shen).

0925-8388/$ – see front matter © 2010 Elsevier B.V. All rights reserved.
doi:10.1016/j.jallcom.2010.06.143

Table 1
Density and elastic characteristics for $Ti_{40}Zr_{25}Ni_3Cu_{12}Be_{20}$ bulk metallic glass.

ρ_0, g/cm^3	C_l, m/s	C_t, m/s	E, GPa	K, GPa	G, GPa	ν
5.44 ± 0.01	5295 ± 10	3180 ± 30	134	79	55	0.218

calculated from the following equations [14]:

$$K = \rho_0 \left(C_l^2 - \frac{4}{3} C_t^2 \right) \quad (1)$$

$$G = \rho_0 C_t^2 \quad (2)$$

$$E = \frac{9KG}{3K + G} \quad (3)$$

$$\nu = \frac{3K - 2G}{6K + 2G} \quad (4)$$

where K is the bulk modulus, G the shear modulus, E the elastic Young's mudulus, and ν the Poisson ratio. The data of aforementioned characteristics are examined and listed in Table 1.

The dynamic strength investigations of the bulk glassy samples were performed by plane plate-impact technology on an electrical explosion of conductor installation (EEC). The glass samples were in the form of plate with a size of 3 mm × 30 mm × 30 mm and the flyers were in the form of a disk, 20 mm in diameter and 1.7 mm in thickness. The parameters of EEC are as follows: capacitance C is 6 μF, voltage U is 50 kV, total energy E is up to 7.5 kJ, short circuit duration T is 11 μs. Velocities of the aluminum impactor range from 250 to 750 m/s, controlled by a differential laser interferometer. Plasma energy generated by explosion of conductors is used for projectile acceleration, allowing the investigations of submicrosecond shock duration within a velocity rate of 1000–1500 m/s. The scheme for spall testing is presented in Fig. 1. The fracture morphology of the tested samples was examined by scanning electron microscope (SEM) and optical microscope (OM) to reveal the deformation and fracture mechanism.

3. Results and discussion

Fig. 2 shows the XRD pattern of the $Ti_{40}Zr_{25}Ni_3Cu_{12}Be_{20}$ alloy, which consists of only a typical broad diffused peak. No evidence of any Bragg crystalline peaks can be observed from the XRD pattern within the detectable limitation of the XRD, typical of a glassy nature.

Fig. 3 shows the interferogram and the corresponding velocity profile at the free surface for $Ti_{40}Zr_{25}Ni_3Cu_{12}Be_{20}$ BMG samples impacted by Al flyer at the impact velocity of 570 m/s. As can be seen from Fig. 3, the free surface particle velocity firstly raised to 300 m/s without a kink, suggesting that only elastic shock wave propagated within the sample and the stress behind the shock front was lower than the HEL stress. Then the free surface particle velocity rapidly dropped down to 90 m/s, followed by a small fluctuation, indicating the occurrence of spallation within the sample under dynamic loading.

Fig. 4 shows a schematic of wave propagation in the flyer and the target BMG sample (t–X diagram) for a typical plate-impact spall

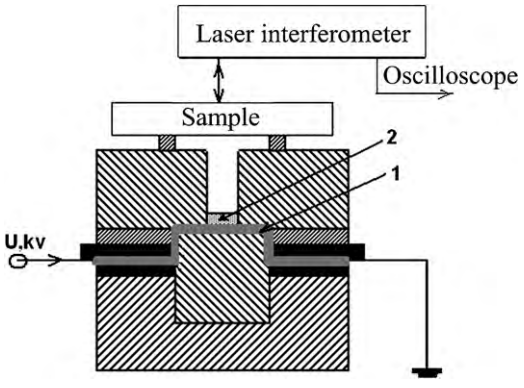

Fig. 1. Schematic illustration of the set-up for spall strength investigation: (1) exploding foil (aluminum foil with dimensions 0.01 mm × 20 mm × 50 mm); (2) plate-flyer from aluminum alloy with dimensions Ø 20 mm × 1.7 mm.

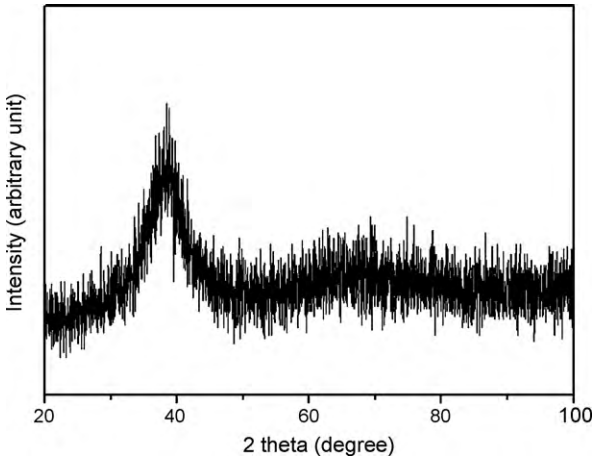

Fig. 2. XRD pattern for the as-cast $Ti_{40}Zr_{25}Ni_3Cu_{12}Be_{20}$ bulk glassy sample.

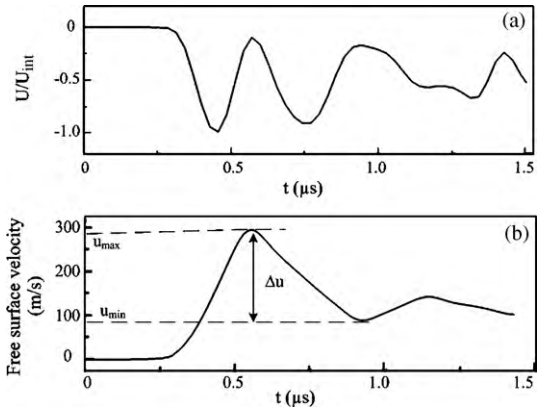

Fig. 3. Interferogram (a) and corresponding free surface velocity profile (b) obtained for $Ti_{40}Zr_{25}Ni_3Cu_{12}Be_{20}$ glassy samples impacted by Al flyer at the impact velocity of 570 m/s.

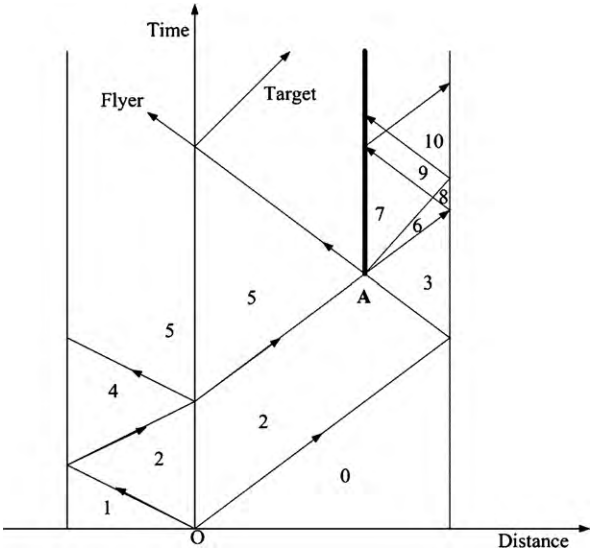

Fig. 4. Wave propagation in the flyer and the target BMG sample (X–t diagram) for a typical plate-impact spall experiment. The arrows indicate the direction of wave propagation.

experiment. The horizontal coordinate represents the distance in the target and the flyer from the impact surface, while the longitudinal coordinate represents the time after impact. As shown in Fig. 4, upon impact, compressive waves are generated in both the target and the flyer plates. After reflected from the free surface of the flyer or target BMG, compressive waves would change into the rarefaction waves and propagate to an opposite direction. When the rarefaction waves reflected from the free surfaces of the flyer and the sample interacts at a pre-determined location, A, within the BMG sample, the sample begins to subject to tensile stress. As we know, for a material, when the tensile stress reaches a level beyond its ability to resist decohesion, it fails in a process known as spallation (Region 7). The material's spall strength can be calculated by the following equation [13]:

$$\sigma_{\text{spall}} = \frac{1}{2}\rho_0 C_l \Delta u \tag{5}$$

where Δu can be calculated by the difference between the free surface particle velocity $u_{\max}$ and $u_{\min}$, which can be obtained from free surface velocity profile shown in Fig. 3 (b). According to Eq. (5), the corresponding value of spall strength for $Ti_{40}Zr_{25}Ni_3Cu_{12}Be_{20}$ glassy samples can be estimated to be 2.9 GPa.

When the stress behind the shock front is less than the HEL stress of the material, the shock wave velocity could be replaced with the longitudinal wave velocity of the material. The stress and the strain behind the shock front can be evaluated by the below relations [15]:

$$\sigma_x = \rho_0 C_l u \tag{6}$$

$$\varepsilon = \frac{u}{C_l} \tag{7}$$

where u is the particle velocity behind the shock front which is equal to half of the maximum free surface particle velocity. The corresponding values for σ_x and ε are 4.2 GPa and 2.7%, respectively.

Using the von Mises yield criterion, the yield strength, Y_0, under uniaxial stress loading can be readily computed by the following expression [15]:

$$Y_0 = \frac{1-2\nu}{1-\nu}\sigma_{\text{HEL}} \tag{8}$$

Considering that σ_x is below the HEL stress of the material in this study, replacement of σ_{HEL} with σ_x into Eq. (8) gives:

$$Y_0 > \frac{1-2\nu}{1-\nu}\sigma_x \tag{9}$$

Using the ambient value of ν, accordingly, Y_0 of the glassy alloy studied is larger than 3.0 GPa. For comparison, the quasistatic compression tests on the Ti-based alloy with the same composition gives $Y_0 = 1.8$ GPa [16]. Such discrepancies in the yield strength obtained from different types of loading have been previously observed in Zr-based glass, for which the yield strength obtained from plate-impact experiments (uniaxial strain) and quasistatic compression experiment (uniaxial stress) are 2.83 and 1.9 GPa, respectively [9,17].

After the dynamic loading experiment, the soft-recovered samples were observed under SEM. Fig. 5 shows the typical SEM micrograph for free surface of the shocked sample. Many cracks and shear bands can be observed on the free surface of the shocked sample. The similar phenomenon had been observed on the free surface of a shocked $Zr_{41.5}Ti_{13.5}Cu_{12.5}Ni_{10}Be_{22.5}$ BMG [8]. Zhuang et al. attributed the formation of the shear bands and cracks on the free surface of the shocked sample to the shear localization within the sample during the shock loading.

To characterize the damage area around the spall plane of the $Ti_{40}Zr_{25}Ni_3Cu_{12}Be_{20}$ BMG, the cross-section of the shocked samples were observed. Fig. 6 shows the typical cross-section optical

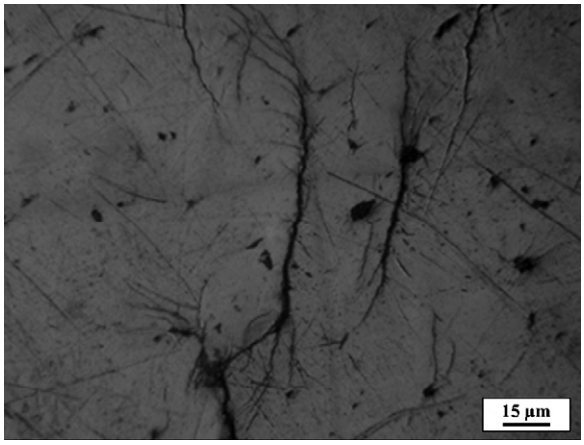

Fig. 5. Typical free-surface SEM micrograph of the recovered $Ti_{40}Zr_{25}Ni_3Cu_{12}Be_{20}$ BMG sample after shock loading.

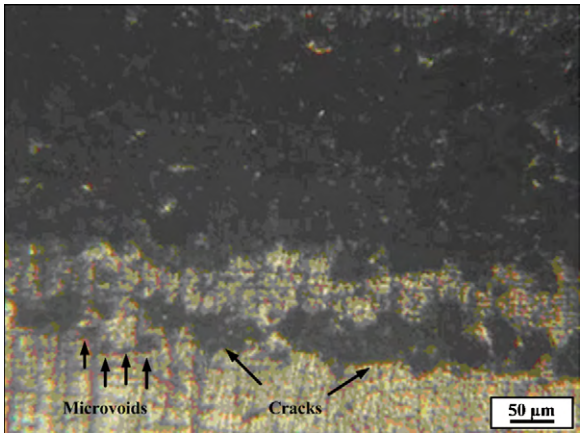

Fig. 6. Typical cross-section OM micrograph of the recovered $Ti_{40}Zr_{25}Ni_3Cu_{12}Be_{20}$ BMG sample showing the damage area around the spall plane.

microscope image of the recovered Ti-based BMG sample. Cracks, which lead to the occurrence of the spallation, can be clearly seen in the damage area around the spall plane. Careful examination reveals that the cracks are formed due to the coalescence of microvoids, as indicated by arrows in Fig. 6. Therefore, the spall plane was formed due to the growth and coalescence of those microvoids.

Based on the Turnbull–Cohen's free-volume theory [18] and Spaepen's model [19], Liu et al. concluded that the free-volume concentration is strongly sensitive to the strain rate, i.e. increasing strain rate could result in a significant increase in the free-volume concentration [20]. Under the shock wave loading, a large number of free volumes would be created in the amorphous alloy due to extremely high strain rate (higher than $10^4\ s^{-1}$). The free volumes in the pre-determined location, A, as marked in Fig. 4, where the rarefaction waves interacts, would spontaneously coalescence to microvoids due to the tensile stress. The local increase in microvoids has been suggested as the main mechanism for nucleation of cracks [21]. Once the cracks nucleate, they will propagate rapidly, therefore, causing the spallation of the sample. Thus, lots of microvoids and cracks could be seen in the damage area around the spall plane of the sample, as shown in Fig. 6.

4. Conclusions

From the results discussed above, several conclusions can be drawn as follows:

(1) Spallation of the Ti-based bulk metallic glass in dynamic loading occurs prior to yielding.
(2) The yield strength of the Ti-based metallic glass under the dynamic loading is larger than the reported quasistatic value.
(3) Cracks and microvoids, which caused the occurrence of the spallation of the sample, are distributed on the cross-section of the recovered Ti-based BMG sample.

Acknowledgements

This work was financially supported by the National Nature Science Foundation of China under Grant Nos. 50911120084 and 10732010, the Chinese National Hi-Tech Research & Development Program (No. 2007AA03Z518), and the Excellent Youth Foundation of Heilongjiang Province under grant no. JC200806.

References

[1] A. Inoue, W. Zhang, T. Zhang, K. Kurosaka, Acta Mater. 49 (2001) 2645.
[2] W.L. Johnson, MRS Bull. 24 (1999) 42.
[3] W.H. Wang, C. Dong, C.H. Shek, Mater. Sci. Eng. R 44 (2004) 45.
[4] M.F. Ashby, A.L. Greer, Scripta Mater. 54 (2006) 321.
[5] A. Inoue, Acta Mater. 48 (2000) 279.
[6] J. Jayaraj, Y.C. Kim, K.B. Kim, H.K. Seok, E. Fleury, J. Alloys Compd. 434–435 (2007) 237.
[7] S.J. Pang, C.H. Shek, K. Asami, A. Inoue, T. Zhang, J. Alloys Compd. 434–435 (2007) 240.
[8] S. Zhuang, J. Lu, G. Ravichandran, Appl. Phys. Lett. 80 (2002) 4522.
[9] S.J. Turneaure, J.M. Winey, Y.M. Gupta, Appl. Phys. Lett. 84 (2004) 1692.
[10] S.J. Turneaure, J.M. Winey, Y.M. Gupta, J. Appl. Phys. 100 (2006) 063522.
[11] T. Mashimo, H. Togo, Y. Zhang, Y. Uemura, T. Kinoshita, M. Kodama, Y. Kawamura, Appl. Phys. Lett. 89 (2006) 241904.
[12] H. Togo, Y. Zhang, Y. Kawamura, T. Mashimo, Mater. Sci. Eng. A 449–451 (2007) 264.
[13] F.P. Yuan, V. Prakash, J.J. Lewandowski, J. Mater. Res. 22 (2007) 402.
[14] L.L. Wang, Foundation of Stress Waves, National Defence Industry Press, Beijing, 2005 (in Chinese).
[15] H. Tan, Introduction to Experimental Shock-Wave Physics, National Defence Industry Press, Beijing, 2007 (in Chinese).
[16] Y.J. Huang, J. Shen, J.F. Sun, Appl. Phys. Lett. 90 (2007) 081919.
[17] Z.F. Zhang, F.F. Wu, G. He, J. Eckert, J. Mater. Sci. Technol. 23 (2007) 747.
[18] D. Turnbull, M.H. Cohen, J. Chem. Phys. 34 (1961) 120.
[19] F. Spaepen, Acta Metall. 25 (1977) 407.
[20] L.F. Liu, L.H. Dai, Y.L. Bai, B.C. Wei, J. Non-Cryst. Solids 351 (2005) 3259.
[21] Y.F. Xue, H.N. Cai, L. Wang, F.C. Wang, H.F. Zhang, Mater. Sci. Eng. A 473 (2008) 105–110.